A study on the numerical modelling of UHPFRC-strengthened members

Renaud Franssen[1,2*], *Serhan* Guner[3], *Luc* Courard[2], and *Boyan* Mihaylov[2]

[1]FRIA (F.R.S.-F.N.R.S), National Fund for Scientific Research, Brussels, Belgium
[2]ArGEnCo Department, Research Unit in Urban and Environmental Engineering, University of Liège, Allée de la Découverte 9, Liège (4000), Belgium
[3]Department of Civil Engineering, University of Toledo, 2801 W Bancroft St., MS 307, NI 3021, Toledo, OHIO (43606-3390), USA

Abstract. The maintenance of large aging infrastructure across the world creates serious technical, environmental, and economic challenges. Ultra-high performance fibre-reinforced concretes (UHPFRC) are a new generation of materials with outstanding mechanical properties as well as very high durability due to their extremely low permeability. These properties open new horizons for the sustainable rehabilitation of aging concrete structures. Since UHPFRC is a young and evolving material, codes are still either lacking or incomplete, with recent design provisions proposed in France, Switzerland, Japan, and Australia. However, engineers and public agencies around the world need resources to study, model, and rehabilitate structures using UHPFRC. As an effort to contribute to the efficient use of this promising material, this paper presents a new numerical modelling approach for UHPFRC-strengthened concrete members. The approach is based on the Diverse Embedment Model within the global framework of the Disturbed Stress Field Model, a smeared rotating-crack formulation for 2D modelling of reinforced concrete structures. This study presents an adapted version of the DEM in order to capture the behaviour of UHPFRC by using a small number of input parameters. The model is validated with tension tests from the literature and is then used to model UHPFRC-strengthened elements. The paper will discuss the formulation of the model and will provide validation studies with various tests of beams, columns and walls from the literature. These studies will demonstrate the effectiveness of the proposed modelling approach.

1 Introduction

Around the world, the maintenance of large aging infrastructure is a persistent problem. The amount of time and investments needed for rehabilitation increases permanently. At the same time, solutions for repair are not durable and require frequent inspections. The limited sustainability of rehabilitation techniques raises the price of maintenance and obliges public agencies to focus on the most deteriorated structures while others are ignored. Subsequently, the number of structures which will need repair effort in the future will increase, considering also that a large portion of the current public infrastructure in the western world was built in the 1970's and 80's. All these bridges, tunnels and other critical infrastructure approach the age of 50 years at which major repair measures are usually necessary.

Considering these pressing issues, ultra-high performance fibre-reinforced concretes (UHPFRC) are a promising class of materials in the field of repair, rehabilitation and strengthening of concrete structures [1,2]. They are based on a very fine granulometry of the constituting particles with a small water-to-cement ratio, and also include steel fibres [3]. This composition provides enhanced properties that are very relevant to structural repairs. UHPFRC is characterized by very high strengths in compression (150-300 MPa) [4] and, more importantly, it also exhibits enhanced tension behaviour both in terms of strength and ductility [5]. The steel fibres bridge the cracks and improve the crack control, resulting in a significantly more ductile behaviour than plain concrete. The enhanced tension behaviour can be used for example for the strengthening of existing members with insufficient shear capacity [6]. In addition to these mechanical properties, UHPFRC is also a quasi-impermeable material with high resistance to aggressive environment [7]. This property is very important for the rehabilitation of existing structures as UHPFRC layers can be used to protect the concrete and reinforcement, and in this way offset or completely eliminate subsequent durability issues.

Despite its enhanced properties, the use of UHPFRC for structural strengthening remains relatively limited. A main reason for this is the lack of commonly accepted models and approaches for evaluating the resistance of UHPFRC-strengthened structures. While the awareness among structural engineers about the properties of

* Corresponding author: r.franssen@uliege.be

UHPFRC is growing, significant research is still needed to provide practitioners and authorities with reliable tools for design calculations. It is therefore the purpose of this paper to contribute towards this objective by describing and validating a nonlinear finite element approach. The goal is to use an existing formulation for the behaviour of reinforced and fibre-reinforced concrete (FRC) [8, 9], and to extend its application to reinforced concrete beams and columns strengthened with UHPFRC layers. The validation of the model is performed with 21 tests from 7 experimental studies reported in the literature [10-16].

2 Constitutive models

In this study, two models will be used for the modelling of UHPFRC. The finite element simulations will be based on the Disturbed Stress Field Model (DSFM) for reinforced concrete proposed by Vecchio (2000) [8]. This model is implemented in the non-linear finite element software VecTor2 [17, 18] in a plane-stress formulation. The additional contribution of fibres in the concrete is modelled with the Diverse Embedment Model [9] (DEM) integrated in the DSFM. Therefore, the DSFM in combination with the DEM are used for the modelling of fibre-reinforced concrete structures. In this study, recommendations are provided on how to apply the same formulation to UHPFRC.

2.1. Disturbed stress field model

The DSFM is a smeared rotating crack model that originates from the modified compression field theory for reinforced concrete elements subjected to shear [19]. In the DSFM, the cracks are assumed parallel to the principal compressive stress directions in the concrete, while the principal strain directions deviate from the stress directions due to slip displacements in the cracks. The slip displacements and crack widths are used to calculate aggregate interlock stresses transferred across the cracks. In addition to aggregate interlock, the DSFM also accounts for the tension stiffening and softening of the concrete, compression softening and confinement of the concrete, as well as the yielding of the reinforcement.

2.2 Diverse embedment model for FRC

The DEM is used for modelling the tension behaviour of fibre-reinforced concrete (FRC). The fundamental assumption of the model is that the tensile stresses in the cracks of FRC can be expressed as the sum of a concrete contribution and fibres contribution (Figure 1). This assumption was introduced by Voo and Foster [20] who developed a variable engagement model (VEM) for FRC. The DEM is largely based on this method, but also includes additional phenomena such as the effect of unsymmetrical anchorage of the fibres and hooked fibres. As evident from Figure 1, the models predict that as the crack opens, the tension transferred by concrete diminishes quickly (tension softening) while the fibres get activated and provide a more ductile post-peak behaviour.

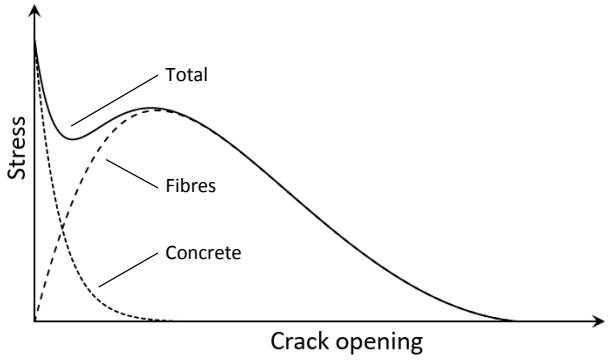

Figure 1. Principle of UHPFRC models (adapted from [20])

While the modelling of the concrete in tension has been established in various codes and recommendations, the DEM defines the participation of the fibres as follows:

$$f_f = \alpha_f V_f \sigma_{f,cr,avg} \quad (1)$$

where f_f is the tensile stress acting on the concrete area and attributed to the fibres, α_f is a factor that accounts for fibre orientation, V_f is the fibre volumetric ratio, and $\sigma_{f,cr,avg}$ is the average fibre stress at the crack. This last quantity is obtained by double integration across all fibre angles θ and embedment lengths l_a:

$$\sigma_{f,cr,avg} = \frac{2}{l_f}\int_0^{l_f/2}\int_0^{\pi/2} \sigma_{f,cr}(l_a,\theta)\sin\theta \, d\theta \, dl_a \quad (2)$$

This model uses a relatively limited number of input properties which do not require any tests other than a standard compression test. The tensile resistance due to the fibres is a function of the fibre diameter, fibre length, steel tensile strength, and the maximal bond strength between the concrete and the fibres. In both the DEM and VEM for straight fibres and regular concrete, the bond strength is defined as $\tau_{f,max} = 0{,}396\sqrt{f_c'}$ [MPa], where f_c' is the compressive strength of the concrete. Concerning UHPFRC, it is proposed to increase the bond resistance in recognition of the high density and high cement content of the UHPFRC matrix. Based on comparisons with tests, the value of $\tau_{f,max}$ is modified to:

$$\tau_{f,max} = 0{,}75\sqrt{f_c'} \quad (3)$$

Figure 2 shows the difference in tensile behaviour of FRC and UHPFRC with identical fibres and fibre ratios (i.e. V_f=1.5%, fibre length = 20 mm and fibre diameter = 0.3 mm) as predicted by the DEM. The compressive strength of the FRC is 50 MPa, while that of the UHPFRC is three times higher. It can be seen that the UHPFRC exhibits higher tensile strength estimated as $0.33\sqrt{f_c'}$. The descending branches of the curves are associated with the pullout behaviour of the fibres, and

therefore depend to a large extend on the bond strength. The bond between the fibres and matrix is stronger for ultra-high performance concrete, and it results in somewhat higher ductility. It should be noted though that the fibres chosen for this comparison are more typical for ultra-high performance fibre reinforced concrete than for FRC. The fibres in FRC are usually longer, thicker, and with lower volumetric ratio.

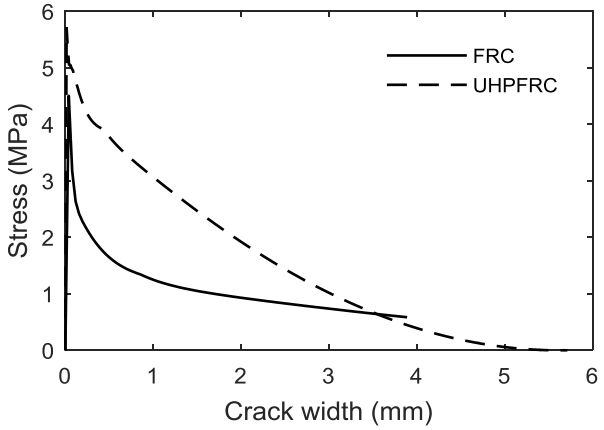

Figure 2. Modelling of FRC and UHPFRC based on the DEM

In the disturbed stress field model formulation (DSFM), the predictions of the DEM are used to evaluate the stresses in the fibre-reinforced concrete in the principal tension direction. However, as the DSFM is a smeared crack approach while the DEM focusses on a discrete crack, it is necessary to establish a relationship between the crack width and the average strains in the concrete. The expression used in the VecTor2 code is [21]

$$w = \left(1.7 + \frac{3.4\, V_f l_f}{d_f}\right) \cdot \varepsilon_1 \cdot s_{cr} \qquad (4)$$

where ε_1 is the average principal tensile strain and s_{cr} is the average crack spacing. The term in the brackets represents the ratio between the maximum crack width and the average crack width measured in FRC tests. The authors of this expression have also proposed an expression for s_{cr} in normal strength members with fibres and conventional reinforcement. However, based on studies of UHPFRC, Jungwirth and Muttoni [22] and Sigrist and Rauch [23] have proposed a simpler expression which is adopted in this paper:

$$s_{cr} = 0.75\, l_f \qquad (5)$$

where l_f is the fibre length. This equation is easy to use and has shown adequate results in the modelling of UHPFRC specimens.

In terms of compression response, the UHPFRC is modelled again on the basis of a model for FRC [24]. In addition to the compressive strength of the concrete, the other important input to the model is the modulus of elasticity which is determined from tests or is assumed equal to 50 GPa.

Finally, as mentioned earlier, the DSFM also accounts explicitly for slip displacements in the cracks. In FRC this slip is associated with aggregate interlock shear stresses across the cracks, but also with tangential stress associated with the fibres. In the modelling of UHPFRC, the aggregate interlock is limited due to the small aggregate size (0.6-1.3 mm), while details about the modelling of the fibre stresses are provided in [25].

3 Modelling of UHPFRC-strengthened beams

In this chapter, the described finite element formulation will be used to model UHPFRC-strengthened beams from the literature. Different strengthening layouts will be considered, i.e. a layer of UHPFRC cast on the compressive side of the section, on the tensile side, or U-shaped layers. In addition, layers with and without conventional steel reinforcement will be modelled.

The study of strengthened beams will first focus on a test series by Safdar et al. [12] which consisted of four specimens with rectangular sections (beam B0, BL20, BL40 and BL60). All beams had identical 400 mm by 250 mm sections reinforced with symmetrical top and bottom longitudinal bars as well as stirrups. The longitudinal reinforcement ratio was 0.44% while the stirrups ratio was 0.31%. The compressive strength of the concrete was 29.7 MPa. The main properties of the concrete members as well as the UHPFRC layers are provided in Table 1.

The beams from the BL series were reinforced with UHPFRC layers cast on the tension side of the section. The only variable of the series was the thickness of the layers. To cast the layers, the concrete at the bottom of the section was removed by water-jetting. Because the thickness of the layers was 0, 20 mm, 40 mm and 60 mm, the longitudinal reinforcement in specimens BL40 and BL60 was respectively partially and fully encased in UHPFRC. The compressive strength of the strengthening material was 156 MPa, the fibre volumetric ratio was 3%, and the fibre length and diameter were respectively 13 mm and 0.16 mm.

The tests specimens were loaded monotonically to failure under symmetrical four-point bending as shown in Figure 3. The length of the two symmetrical shear spans was 1000 mm, resulting in a shear-span-to-effective-depth ratio a/d of 2.8. The control specimen B0, which did not have UHPFRC layers, failed in flexure by yielding of the bottom longitudinal reinforcement and eventual crushing of the concrete at the top of the section.

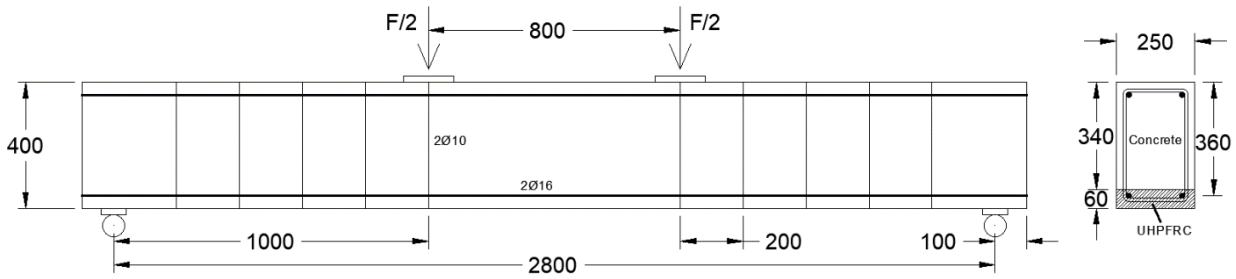

Figure 3. Test setup used by Safdar et al. [12]

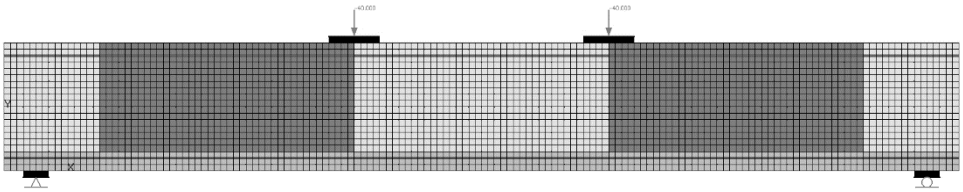

Figure 4. FEM of beam BL60

The finite element model (FEM) of beam BL60 with the thickest UHPFRC strengthening layer is presented in Figure 4. The original concrete and UHPFRC were modelled with quadrilateral elements. The stirrups were represented as smeared vertical reinforcement in the quadrilateral elements, while the top and bottom longitudinal reinforcement was modelled with truss elements. A perfect bond was assumed between the reinforcement and the concrete, as well as between the original member and the strengthening layer. This latter assumption is consistent with the tests results which showed no delamination between the concrete and UHPFRC. The point loads and support reactions were introduced via steel plates which were also modelled with quadrilateral elements. One of the supports was a pin and the other was a roller.

The measured and predicted load-deflection responses of specimens B0, BL20 and BL60 are shown in Figure 5. It can be immediately seen that the FEM captured well the experimental curves, including the initial stiffness , strength and ductility. As mentioned earlier, the control specimen B0 failed in flexure and exhibited a large ductility associated with the yielding of the bottom longitudinal reinforcement. A very similar behaviour was observed in specimen BL20 which had a slightly higher resistance and slightly lower ductility. A further increase of the thickness of the layers from 20 mm (BL20) to 60 mm (BL60) resulted in a substantial stiffness and strength increase, but also in very brittle failures. While the strength increased due to the tensile stresses transferred by the steel fibres across the flexural cracks, the ductility decreased due to the strain localization in the cracks. It was reported that, due to the localization, the failure occurred with rupture of the bottom longitudinal reinforcement in a dominant crack as also predicted by the FEM.

The observed and predicted cracks of the control specimen B0 and the beam with the thickest UHPFRC layer are compared in Figure 6. It can be seen that the two crack patterns differ significantly. While beam BL60 had a single dominant flexural crack, B0 formed a series of parallel cracks. Therefore, for a given deflection, the reinforcement strains in the crack were bigger in the strengthened specimen than in the control beam. The difference in strains is further increased by the difference in bond resistance. As the bottom reinforcement in beam BL60 was encased in the UHPFRC layers, a much higher bond developed along the bars in the vicinity of the cracks. Evan thought this local bond effect is not explicitly modelled in the FEM, the model predicted well the crack patterns of the beams as well as the rupture of the reinforcement in BL60. It is this rupture which caused the sudden drop of resistance in the prediction curve in Figure 5 at a deflection ≈20 mm.

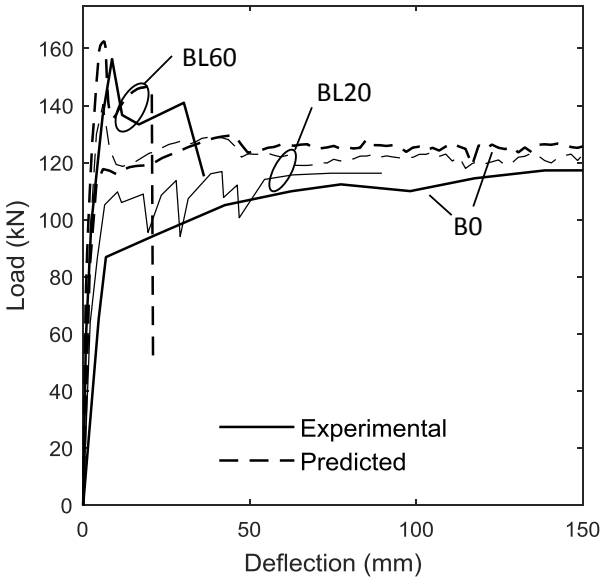

Figure 5. Measured and predicted response of beams with variable thickness of the tension UHPFRC layers (tests [12])

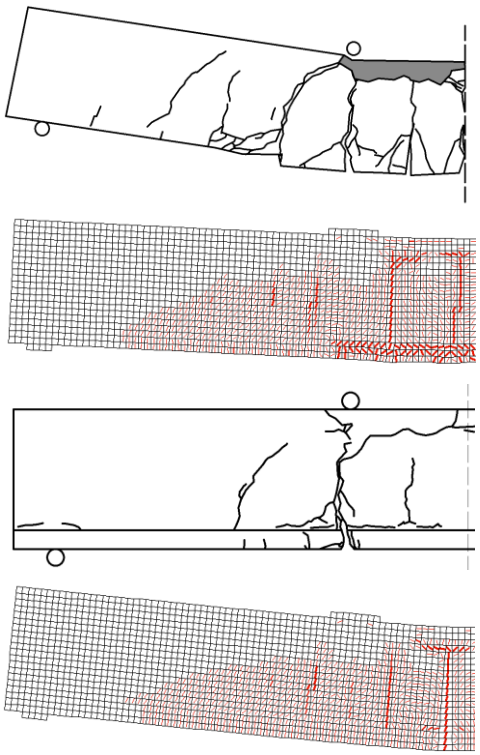

Figure 6. Measured and predicted crack patters at failure of beams B0 (above) and BL60 (below) (post-processor Augustus [26])

Another experimental study that focused on the effect of the thickness of UHPFRC layers was performed by Meda et al. [13]. However, while the beams studied by Safdar et al. [12] had a strengthening layer only on the tension side of the section, the latter test series featured also side layers to increase the durability and shear resistance. The control specimen SR had a 450 mm by 200 mm rectangular section and an a/d ratio of 1.95, see Table 1. There were no stirrups in the beam, and therefore it failed in shear along a critical diagonal crack. The strengthened beams SA and SB featured U-shaped layers with a thickness of 30 mm and 50 mm, respectively. While the thin UHPFRC layers had only steel fibres (V_f=1.25%), the thick layers also included U-shaped transverse reinforcement for higher shear resistance (open stirrups).

The U-shaped UHPFRC layers required somewhat different modelling approach than the layers placed at the top/bottom of the section. Because VecTor2 implements a 2D plane-stress formulation, it was necessary to use overlapping elements for the modelling of the beam web. The web included three layers of elements with coinciding nodes: one layer for the original concrete section and two for the UHPFRC cast on either side of the concrete. Because the model is 2D, possible slip displacements between the concrete and UHPFRC are neglected (perfect bond conditions). In reality, the interface between the two materials was roughened with sandblasting.

Figure 7 shows the measured and predicted responses of beams SR, SA and SB. It can be seen that the control specimen SR, which failed in shear, exhibited a brittle behaviour with a fast drop of resistance in the post-peak regime. The UHPFRC layers suppressed the shear failure, and the two strengthened beams failed in flexure with significant yielding of the bottom reinforcement.

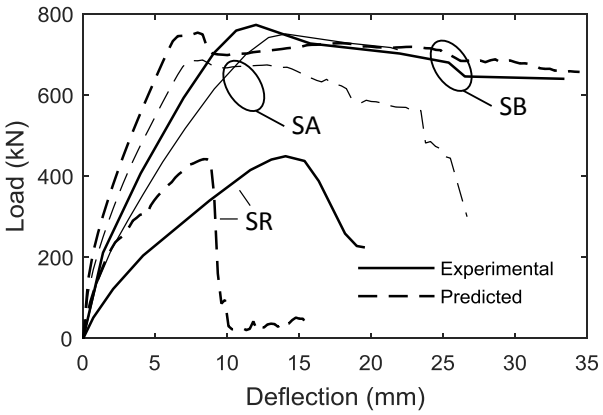

Figure 7. Measured and predicted response of beams with variable thickness of U-shaped UHPFRC layers (tests [13])

As compared to specimen BL60 by Safdar et al. [12], beams SA and SB exhibited a ductile behaviour. This difference is explained mainly by the amounts of longitudinal reinforcement used in the two test series. While BL60 had a reinforcement ratio of only 0.44%, SA and SB had 1.17% and 1.02%, respectively (Table 1). Therefore, the UHPFRC layers in the latter case had a relatively minor contribution to the flexural capacity, and thus a small influence on the ductility. This is confirmed by the fact that, even though specimen SB had significantly ticker UHPFRC layers than SA, the two beams had nearly the same flexural capacity. As evident from Figure 7, the FEM captured well the load bearing capacity of the three beams, even though it overestimated the difference between SA and SB. While SB was predicted to fail in pure flexure, the model predicted a combined flexure-shear failure of beam SA. Also, the model overestimated the stiffness of the beams on the basis of an estimated modulus of elasticity of the concrete of 29900 MPa [13].

Similar FEM analyses were performed on a total of 18 UHPFRC-strengthened beams from the literature [10-14], see Table 1. All comparisons were performed with the same constitutive models (see section 2) without additional calibration of model coefficients. On this basis, the FEM produced beam strength predictions with an average experimental-to-predicted ratio of 1.00 and a coefficient of variation (COV) of 11.12%.

4 Strengthened walls or columns

In addition to beams, this study also includes the modelling of UHPFRC-retrofitted vertical elements such as columns and walls. A typical application of this retrofit technique is found in column- or wall- type bridge piers as these members are often exposed to aggressive environment (i.e. deicing salts). Therefore, the UHPFRC can be used to both protect against corrosion and increase the load-bearing capacity. In these applications the UHPFRC is often applied only in the corrosion-critical zones near the base of the member.

There are two main differences between the UHPFRC strengthening of beams and columns/walls. First, due to the presence of slabs, beams are usually retrofitted with bottom or U-shaped UHPFRC layers. In contrast, columns and walls are almost exclusively retrofitted with UHPFRC jackets that envelope the entire section. Second, there is a difference in the effectiveness of the UHPFRC layers in the critical sections of the members. While in beams the strengthening layers provide a full contribution to the flexural capacity, this is not the case in the base sections of columns and walls where the bending moments are usually maximum. In these locations there is a construction joint between the UHPFRC and the existing foundation, and therefore the steel fibres in the strengthening layers cannot transfer tension to the foundation. As a result, the UHPFRC contributes only to the compression zone of the base section, as well as to the flexural and shear resistance above this section.

These differences were taken into account in the modelling of tests by Garneau [16] that included two bridge piers. The main goal of tests S5 and S6 was to demonstrate that UHPFRC can be used to strengthen deficient lap splices located above the foundation of the pier. The specimens differed in the yield strength of the lapped reinforcement (485 MPa for S5 vs. 405 MPa for S6) as well as the amount and detailing of the transverse reinforcement (seismic vs. non-seismic stirrup design). The dimensions of the original concrete section were 1200 mm by 600 mm, and this section was reduced to 900 mm by 300 mm after water jetting. The full dimensions of the section were recovered by casting a UHPFRC jacket with a compressive strength of 144 MPa and a fibre ratio of 3%, see Table 1. The piers were loaded with a horizontal force applied at 2675 mm above the base, resulting in shear-height-to-depth ratio 2675/1200=2.23. The vertical load on the specimens was kept constant with a value of 6% of the compressive capacity of the original concrete section.

The finite element model of the specimens is shown in Figure 8. It includes both the test region and the foundation block which was significantly ticker (2000 mm). As the longitudinal reinforcement was distributed across the entire section, it was modelled as smeared reinforcement similarly to the stirrups.

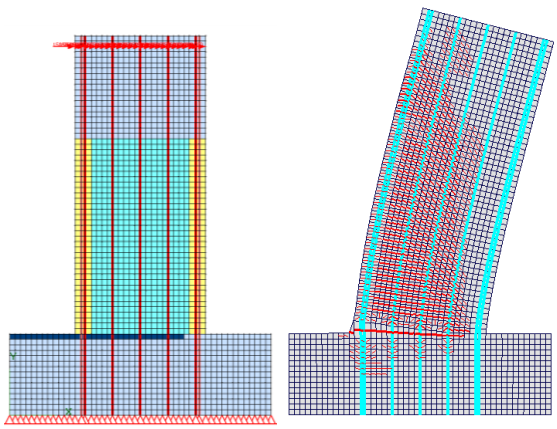

Figure 8. Finite element model and predicted crack pattern at failure of column S5

The UHPFRC layers were modelled in the same way as that was done for the beams with U-shaped layers, except that an additional layer was added on the compression edge of the pier. To avoid an unrealistic transfer of tensile stresses from the fibres to the foundation block, the top row of elements in the foundation was modelled with a smaller thickness across the tension zone of the base section. The depth of the tension zone at failure was estimated iteratively based on several analyses and a trial and error procedure.

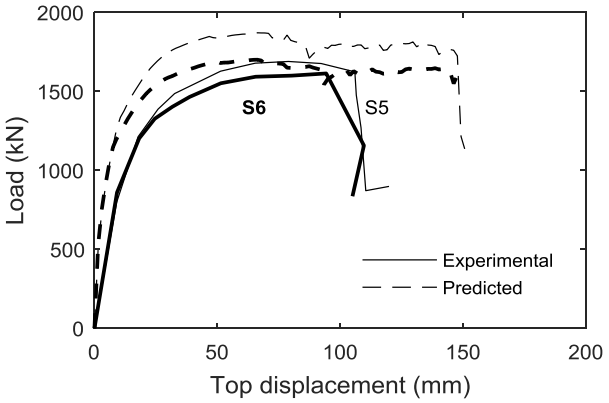

Figure 9. Measured and predicted response of columns with UHPFRC jackets (tests [16])

As evident from Figure 8, this modelling resulted in a wide crack in the base section where the fibres were not effective. Large plastic deformations developed in the longitudinal reinforcement in this section, while the remaining part of the pier remained largely elastic. The same observations were reported in the tests where the failure was eventually caused by the rupture of the reinforcement in the base crack. The UHPFRC layers were sufficient to completely suppress lap-splice failures.

As can be seen from Figure 9, both tests specimens behaved very similarly in terms of lateral load vs. top lateral displacement. They exhibited significant ductility before the reinforcement ruptured. Specimen S5 was slightly stronger than S6 due to the higher yield strength of the reinforcement. It can also be seen that the FEM captured well the experimental results, even though it overestimated the displacement corresponding to steel rupture.

The last comparisons in this study are performed with three column tests performed by Meda et al. [15]. The tests specimens with a 300 mm by 300 mm original concrete section featured similar support and loading conditions as piers S5 and S6. The axial load was constant and corresponded to 26% of the compression capacity of the original concrete section. Prior to testing to failure, two of the original columns were subjected to accelerated corrosion, which resulted in an approximately 20% reduction of the mass of the longitudinal reinforcement as well as partial spalling of the concrete cover. The main properties of the specimens are summarized in Table 1.

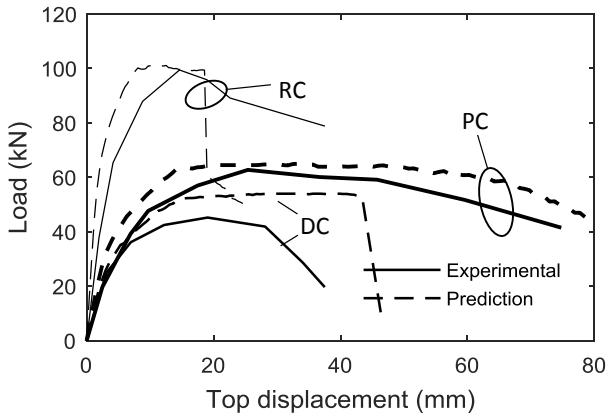

Figure 10. Measured and predicted response of corroded and repaired columns (tests [15])

Figure 10 shows the measured and predicted responses of the three columns. Specimen PC is the original reinforced concrete column which was not subjected to corrosion. The accelerated corrosion was applied to specimens DC and RC, where the former column was tested without repair while the latter was provided with a 40mm-thick UHPFRC jacket. All specimens failed in flexure at the base section, but exhibited different strengths and ductility. As compared to the undamaged specimen PC, the corrosion in specimen DC resulted in a substantial decrease of both strength and ductility. By applying a UHPFRC jacket on specimen RC, the strength was increased significantly while the ductility remained small as compared to the original column without corrosion. The FEM captured very well the behaviour of specimens PC and RC, and slightly overestimated the load and displacement capacity DC. This is devoted to uncertainties of the properties of the corroded reinforcement (distribution of the corrosion in the section and along the bars) and the surrounding damaged concrete (splitting cracks and partially spalled concrete cover).

Finally, Figure 11 summarizes the strength predictions of all 21 specimens with UHPFRC layers included in this study. On the horizontal axis is the ratio of the thickness of the UHPFRC layer to the total depth of the section parallel to the plane of loading. On the vertical axis is the experimental-to-predicted failure load of the test specimens. As evident from the plot, the data points are grouped close to the unit line across the entire range of t/h values, thus exhibiting no clear bias with respect to this variable. The average experimental-to-predicted ratio is 0.99 and the COV is 11.2%.

5 Conclusions

This study demonstrated that FE modelling based on the disturbed stress field model and the diverse embedment model is a valuable approach for the assessment of UHPFRC-strengthened concrete members. While these models were originally developed for reinforced concrete and fibre-reinforced concrete, it was shown that they can be easily extended to model UHPFRC strengthening layers. The advantage of these models is that they require a straightforward input without unknown parameters to define the behaviour of ultra-high performance concrete.

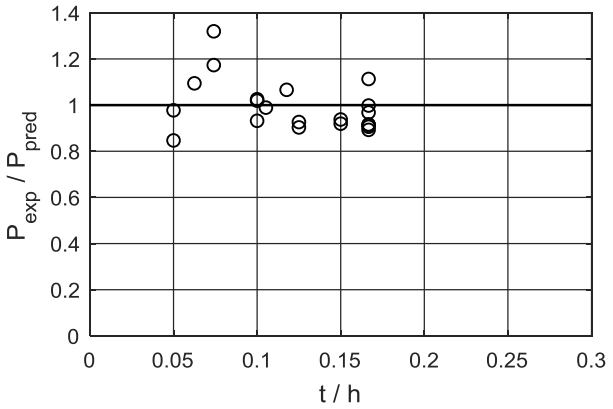

Figure 11. Experimental-to-predicted ratios for 21 beams and columns with strengthening UHPFRC layers

The results from the comparisons with both beam and columns tests showed adequate strength predictions without a clear bias with respect to important tests variables. Because the models were built on an existing formulation and FE code, they can be easily applied by engineers who are already familiar with the formulation for reinforced and fibre-reinforced concrete. As the modelling of UHPFRC is an obstacle to the application of this durable retrofitting material, the FEMs presented in this study represent a step towards removing these difficulties.

References

1. K. Habel, E. Denarié, E. Brühwiler, J. Struct. Eng., **132**, No. 11, 1793-1800 (2006)
2. E. Brühwiler, E. Denarié, Struct. Eng. Int., **23**, No. 4, 450-457 (2013)
3. H.G. Russell, B.A. Graybeal, U.S. Department of Transportation, McLean, VA, Report No. FHWA-HRT-13–060 (2013)
4. K. Wille, A.E. Naaman, G.J. Parra-Montesinos, ACI Mater. J., **108**, No. 1, 46–54 (2011)
5. T Leutbecher, E. Fehling, Internation Symposium on UHPC, Kassel, 435-448 (2004)
6. M. Bastien-Masse, E. Brühwiler, Struct. Eng. Int., **26**, No. 4, 365-374 (2016)
7. S. Abbas, M. L. Nehdi, M. A. Saleem, IJCSM, **10**, No. 3, 271-295 (2016)
8. F.J. Vecchio, J. Struct. Eng., **97**, No. 1, 102-110 (2000)
9. S.-C. Lee, J.-Y. Cho, F.J. Vecchio, ACI Struct. J., **108**, No. 5, 516-525 (2011)
10. F.J. Alaee, B.L. Karihaloo, J. Compos. Constr., **7**, No. 3, 174-186 (2003)
11. T. Noshiravani, PhD Thesis at École Polytechnique Lausanne, Switzerland, *Structural Response of R-*

UHPFRC – RC Composite Members Subjected to Combined Bending and Shear (2004)

12. M. Safdar, T. Matsumoto, K. Kakuma, Compos. Struct., **157**, 448-460 (2016)
13. A. Meda, S. Mostosi, P. Riva, ACI Struct. J., **111**, No. 5, 1059-1068 (2014)
14. G. Martinola, A. Meda, G.A. Plizzari, Z. Rinaldi, Cem. Concr. Compos., **32**, 731-739 (2010)
15. A. Meda, S. Mostosi, Z, Rinaldi, P. Riva, Mater. Struct., **49**, 1967-1978 (2016)
16. J.-F. Garneau, PhD Thesis at École Polytechnique de Montréal, Canada, *Réhabilitation sismique des piles-murs de pont rectangulaires par chemisage en béton fibré à ultra-haute performance* (2015)
17. P. Wong, H. Trommels, F.J. Vecchio, VecTor2 and FormWorks Manual (2013)
18. P. Wong, H. Trommels, F.J. Vecchio, VecTor2-Software for nonlinear analysis of two-dimensional reinforced concrete membrane structures (2014)
19. F.J. Vecchio, M.P. Collins, ACI J. Proc., **83**, No. 2, 219-231 (1986)
20. J.Y.L. Voo, S.J. Foster, Uniciv Report No. R-420, School of Civil and Environmental Engineering, University of New South Wales, 86 pp (2003)
21. J.R. Deluce, S.-C. Lee, F.J. Vecchio, ACI Struct. J., **111**, No.1, 93-102 (2014)
22. J. Jungwith, A. Muttoni, Proceedings of the International Symposium on Ultra High Performance Concrete in Kassel, Germany, 533-546 (2004)
23. V. Sigrist, M. Rauch, Tailor Made Concrete Structures - Walraven & Stoelhorst (eds), 405-410 (2008)
24. S.-C. Lee, J.-H. Oh, J.-Y. Cho, Materials, **8**, No. 4, 1442-1458 (2015)
25. S.-C. Lee, J.-Y. Cho, F.J. Vecchio, ACI Struct. J., **113**, No. 2, 275-285 (2016)
26. E.C. Bentz. Ph.D. thesis, Department of Civil Engineering, University of Toronto, Toronto, Canada, *Sectional Analysis of Reinforced Concrete Members* (2000)

Table 1. Tests specimens

	Author	Name	b (mm)	h (mm)	t (mm)	d (mm)	a/d	f'_c (MPa)	$f'_{c,UHPFRC}$ (MPa)	V_f (%)	ρ_l (%)	ρ_v (%)	V_{exp} (kN)	V_{pred} (kN)	V_{exp}/V_{pred}	UHPFRC layout
1	Alaee	Mix1_st2_20	100	170	20	130	2.7	47	207	6	1.33	0.87	58	54.4	1.07	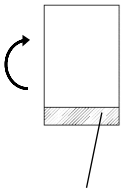
2	Noshiravani	BMW0	150	250	0	237	3.4	41.6	0	0	0.67	0.34	43.2	46.6		
3		BMW1	150	300	50	237	3.4	41.6	160	3	0.67	0.17	58.9	65	0.91	
4		BMW2	150	300	50	255	3.1	41.6	160	3	1.16	0.17	104.7	104.9	1.00	
5		BMW3	150	300	50	252	3.1	41.6	160	3	1.04	0.17	91.7	100.3	0.91	
6		BMW4	150	300	50	255	3.1	41.6	160	3	1.16	0.17	90.7	101.6	0.89	
7		BMW5	150	300	50	255	3.1	41.6	160	3	1.16	0.17	99.6	108.7	0.92	
8		BMN1	150	300	50	255	3.1	41.6	160	3	1.16	0.34	96.7	99.9	0.97	UHPFRC
9		BMN3	150	300	50	248	3.2	41.6	160	3	1.68	0.34	134.7	121	1.11	
10	Safdar	B0	250	400	0	360	2.8	29.7	0	0	0.44	0.31	118.9	129.45		
11		BL20	250	400	20	360	2.8	29.7	156	2	0.44	0.31	118.9	140.4	0.85	
12		BL40	250	400	40	360	2.8	29.7	156	2	0.44	0.31	145.3	155.9	0.93	
13		BL60	250	400	60	360	2.8	29.7	156	2	0.44	0.31	156.3	166.7	0.94	
14		BU20	250	400	20	360	2.8	29.7	156	2	0.44	0.31	142.2	145.5	0.98	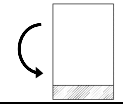
15		BU40	250	400	40	360	2.8	29.7	156	2	0.44	0.31	148.2	145.4	1.02	
16		BU60	250	400	60	360	2.8	29.7	156	2	0.44	0.31	137	149	0.92	
17	Meda	SR	200	450	0	410	1.95	32.6	0	0	1.5	0	450	442		
18		SA	260	480	30	410	1.95	32.6	108	1.25	1.17	0	751	686.3	1.09	
19		SB	300	500	50	410	1.95	32.6	105	1.25	1.02	0.09	773	753.8	1.03	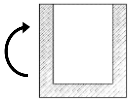
20	Martinola	Control	300	500	0	460	2.37	22	0	0	0.3	0	190	146.294		
21		Reinf.	380	540	40	460	2.37	22	177	2.5	0.3	0	407.8	309	1.32	
22		No-Reinf.	380	540	40	540	2.01	22	177	2.5	0	0	257.2	219.2	1.17	
23	Meda	PC	300	300	0	260	5.77	17	0	0	0.51	0.11	63	61		
24		DC	300	300	0	260	5.77	17	0	0	0.41	0.11	46	54.2		
25		RC	380	380	40	300	45	17	130	1.2	0.28	0.09	100	101.1	0.99	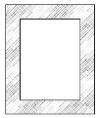
26	Garneau	S5	600	1200	150	945	2.83	36	144	3	0.8	0.33	1690	1871	0.90	
27		S6	600	1200	150	945	2.83	35	142	3	0.8	0.11	1576	1701	0.93	
														Average	**0.99**	
														COV (%)	**11.21**	

b= width of retrofitted section; h= depth of retrofitted section; t= thickness of UHPFRC layers; d=effective depth of retrofitted section based on the longitudinal reinforcement in the tension ½ of the section (i.e. within h/2 from the tension edge); a= span/height of the beam/column subjected to constant shear; f'_c= compressive strength of concrete; $f'_{c,UHPFRC}$ = compressive strength of UHPFRC;

V_f= fibre volume ratio of the UHPFRC; ρ_f= A_s/bd= longitudinal reinforcement ratio (A_s is the reinforcement within h/2 from the tension edge of the section); ρ_v= stirrup ratio calculated with regards to width b.